JOURNAL OF PROPULSION AND POWER
Vol. 17, No. 2, March–April 2001

Near-Field Ion Energy and Species Measurements of a 5-kW Hall Thruster

Frank S. Gulczinski, III* and Alec D. Gallimore†
University of Michigan, Ann Arbor, Michigan 48109

A molecular beam mass spectrometer has been used to determine the ion composition and energy distribution of the P5 5-kW class laboratory Hall thruster. A skimmer was used to obtain a sample of the plasma 10 cm downstream of the thruster exit plane. The thruster was operated at several discharge conditions and rotated with respect to the sampling skimmer in order to determine ion-energy profiles at various plume angles. These measurements were compared to data taken 75 cm from the discharge plane to examine the evolution of the ion-energy profile and facility effects. Both ion-energy measurements and time-of-flight mass spectroscopy revealed evidence of singly, doubly, triply, and quadruply charged xenon ions within the plume. Ion-energy distributions were used to determine that the P5's magnetic field is oriented such that the plume has an overall inward focus. The ion-energy distributions taken 10 cm from the thruster had smaller full width at half maxima and less evidence of elastic collisions than those taken at 75 cm. Comparisons made with laser-induced fluorescence data showed good agreement.

Introduction

PREVIOUS Hall-thruster research concentrated primarily on the 1.5-kW class of thrusters because they were of primary interest for commercial and military satellite use. However, driven by industry trends and IHPRPT (integrated high payoff rocket propulsion technology) goals, the Hall-thruster market is expanding beyond the 1.5-kW class to both sub-kW thrusters for small satellites and high-power thrusters for orbit transfer missions. Of particular interest for orbit-transfer missions are 5-kW-class thrusters. The University of Michigan, in conjunction with the U.S. Air Force, has developed a 5-kW class Hall thruster for basic research purposes. This thruster, the P5, underwent performance and probe testing[1] that indicated it operates in a manner consistent with thrusters under commercial development.[2–4] Its purpose is to serve as a test bed for the development of diagnostics, investigations of Hall-thruster physics, studies of spacecraft interaction issues, and development of next-generation electric propulsion devices.

The configuration of three-axis-stabilized communication satellites is such that the part of the plume of a Hall thrusters used for North/South station keeping (NSSK) will impact the solar arrays of the spacecraft. This can have a negative impact on spacecraft operations and life. Sputtering-induced erosion of antireflective solar-cell cover glass coatings can degrade solar-array performance by a few percent.[5] Erosion of solar-cell interconnects can increase the resistivity of the array circuit and reduce array performance. Although researchers have relied on sample exposure tests and computational modeling to predict the impact that plume impingements on spacecraft solar array material will have on spacecraft operations, these efforts have been hampered by facility effects and the need to make simplifying assumptions about the plume.[5,6] This may lead to large uncertainties at best and serious underprediction of solar-array erosion at worst.

Researchers in the past have shown that Hall-thruster plumes consist of multiply charged ions.[7] The production of multiply charged ions in the thruster discharge chamber not only represents a loss mechanism in terms of thrust, efficiency, and mass utilization[8] but also causes more damage to the discharge chamber walls and adjacent spacecraft surfaces as a result of the higher energy of the multiply charged ions. Therefore, it is essential that the distribution of the energy and charge state of the plume ions is measured and incorporated into the appropriate models to make a more accurate assessment of solar-array erosion.

In spite of the importance of $f(E_i)$ (ion-energy distribution function) for determining ion transport properties, there are only a few direct measurements of $f(E_i)$. The most commonly used device for measuring the ion-energy distribution function is the retarding potential analyzer (RPA).[9] However, the raw RPA data must be differentiated numerically to obtain the energy distribution, and thus the noise of the raw data is magnified when the resulted distribution curves are calculated. Furthermore, the RPA technique cannot distinguish different ion species in the thruster plume. Thus, our investigation has concentrated on using species-differentiating techniques in characterizing Hall-thruster plumes.

In this work the Plasmadynamics and Electric Propulsion Laboratory's (PEPL) molecular beam mass spectrometer[10] (MBMS) was used to investigate the ion energy and charged species composition of the P5. The purpose of this work was threefold. First, the test facility had undergone a pumping upgrade since earlier MBMS tests. This lowered the pressure during testing, thereby reducing the collision frequency between plume ions and background neutral particles. Second, flexibility in choosing the operating conditions of this thruster allowed for testing at multiple operating points. Third and most important, the MBMS was modified to allow near-field measurements to be taken by placing a sampling orifice 10 cm away from the discharge plane of the thruster. This provided information on the evolution of ion energy and charge state profiles, as well as on facility effects. These measurements should be of great use in all aspects of thruster design and research. It addresses integration concerns by providing a method to create a straightforward map of ion concentration, energy, and charge state in the plume of the Hall thruster. It also provides an understanding of the ion acceleration process by taking measurements at multiple axial points to provide ion vectors. This will allow thruster designers the opportunity to examine the effect that changes that they make in thruster configuration have on the ion acceleration structure. These ion vector measurements should also be valuable to thruster modelers, by allowing them to compare their ion acceleration structures directly with those determined experimentally.

Presented as Paper 99-2430 at the AIAA/IASME/SAE/ASEE 35th Joint Propulsion Conference and Exhibit, Los Angeles, CA, 20–24 June 1999; received 7 August 1999; revision received 15 October 2000; accepted for publication 25 October 2000.

*Graduate Student, Department of Aerospace Engineering, FXB Building; currently Research Scientist, Air Force Research Laboratory, AFRL/PRRS, Edwards AFB, CA 93524-7013. Member AIAA.

†Associate Professor, Department of Aerospace Engineering, FXB Building. Associate Fellow AIAA.

Experimental Setup

Tests were performed in PEPL's 6 × 9 m Large Vacuum Test Facility (LVTF), which is pumped by four CVI model TM-1200 Re-Entrant Cryopumps. They provide a measured xenon pumping speed of 140,000 l/s with a base pressure of 2×10^{-7} torr. Pressure was determined by averaging the measurements of two ion gauges, with a calibration factor of 2.87 used to correct for xenon.[11] These gauges were located on the side wall of the LVTF, approximately 2.5 m laterally from the P5 and 2 m and 5 m behind it. Propellant flow was controlled by two MKS model 1100 flow controllers, which were calibrated using a known volume and the ideal gas law corrected for the compressibility of xenon.

Laboratory supplies were used to provide power to the P5. The discharge circuit was electrically isolated during operations. A filter consisting of 1.3-Ω equivalent resistance in series with the discharge current and a 95-μF capacitor in parallel was used to dampen thruster oscillations.

The MBMS is a time-of-flight mass spectrometer with a 45-deg parallel-plate energy analyzer. It is essentially two instruments in one, which when used together can give direct measurements of both ion energy and species composition. Mounted to one end of the LVTF, ions pass into the MBMS through a sampling orifice. The beam enters the 45-deg energy analyzer with length l and width d, which allows only ions of a specific energy-to-charge ratio E/qe to pass through and reach the detector. This ratio is selected by setting the pass voltage V_p between the plates of the analyzer according to the following equation:

$$V_p/(E/qe) = 2d/l \tag{1}$$

By sweeping the value of this pass voltage, an ion energy distribution function can be determined. The MBMS is pumped by two diffusion pumps and, in near-field mode, a turbopump in addition to the LVTF pumps. This ensures that the pressure in the MBMS is lower than in the LVTF, minimizing the probability of collisions within the device relative to the plume.

Uncertainties in ion-energy distributions lie in four areas. Foremost is the effect of collisions on the distributions. These are of critical importance to the understanding of plume composition and will be discussed in greater detail in a subsequent section. There is also uncertainty in the gain of the MBMS in the conversion of the detector signal, a ceramic electron multiplier (CEM), to ion current. The CEM is an ion detector, which produces an output current proportional to the number of ion impacts. This output current was measured using a Keithley model 486 picoammeter that had an overall range of 2 fA to 2 mA. The accuracy of the picoammeter varied with measurement range: ±0.3% at 2 nA, ±0.2% at 20 nA, and ±0.15% at 200 nA and 2 μA. The third area of uncertainty arises because the slits of the MBMS are of finite width, which allows ions with non-nominal trajectories to reach the detector. By properly setting the dimensions of the MBMS, the spread in ions admitted to the detector for a given ion energy is kept to 0.4% of that ion energy.[12] The final possible source of uncertainty is the possibility of charging of the MBMS through ion impact. Because the ion pass voltage is measured relative to the MBMS, drift away from ground would affect the measured ion energy. However, the MBMS is grounded to the LVTF, which is an excellent ground source because of its size. Measurements do not show a drift in the charge of the MBMS when the thruster is fired.

For species composition the time-of-flight mass spectrometer is used. This is the same physical system, with an electrostatic beam gate placed downstream of the sampling orifice. By pulsing the gate open and recording the time it takes for the ions to reach the detector, the individual species of the plasma can be identified because the Hall thruster accelerates them to different velocities based on their charge state. Because their velocities are different, they will arrive at the detector at different times. In addition to the uncertainties discussed for the ion-energy measurements, time-of-flight measurements have uncertainty in the travel time. If a complex, multielement plasma were being interrogated, this could cause uncertainty in the identification of the constituent ions. Fortunately, the Hall-thruster plume consists only of xenon, and in all cases these appeared at, or very close to, the expected value of ion mass/unit charge. The maximum uncertainty was approximately ±5 amu. An additional item that should be noted is that because of the large gains required for these measurements, some traces showed electronic ringing following the most intense peaks (as seen later in Fig. 9 for Xe^+). References 10 and 12 provide more detail regarding the theory and development of the 45-deg energy analyzer and the time-of-flight system.

For measurements 75 cm from the thruster exit plane, the system was configured as shown in Fig. 1a, with the P5 mounted on a rotary-positioning table that allowed it to be rotated with respect to the sampling orifice. For these measurements the center of rotation was the center of the thruster exit plane. Ion-energy measurements were taken in 5-deg increments from 0 deg until loss of signal in one direction only. The 45-deg pass voltage was swept from 0 to 1000 V in 1 V increments by a Keithley model 2410 SourceMeter. This sourcemeter had a rated accuracy of better than 0.012% over the full range of interest. Because of the nature of the energy analyzer,[10] this pass voltage sweep results in a sweep of ion energy of 0 to 1800 eV. Because the signal intensity drops off rapidly away from centerline, species composition measurements were taken at 0° only. Time-of-flight measurements were taken at the peak ion energy, as determined using the 45-deg energy analyzer, and in 20-V increments above and below that voltage. The time-of-flight path length was 2.34 m.

For near-field measurements 10 cm from the thruster exit plane, an extension to the system was built, as shown in Fig. 1b. For these measurements the center of rotation was the center of the annular discharge chamber. This was done so that the ion-energy contributions of one side of the discharge chamber could be examined independently of the other to minimize the detection of crossover flow. Ion energy and species composition measurements were performed at the same angles as the far field (relative to the new center of rotation) and over the same range as for far-field measurements. For the near-field measurements the time-of-flight distance increased to 2.92 m as a result of the use of a miniaturized gate near the sampling skimmer.

Experimental Results

For both the near and far field ion energy and species composition data were taken at two thruster operating conditions. These conditions are summarized in Table 1 along with the LVTF pressure. For comparison, during King's tests on the SPT-100 the maximum chamber pressure was 5×10^{-5} torr. Condition 1 will be referred to as "low voltage" and condition 2 will be referred to as "high voltage."

When examining the ion-energy results, we expect to see the telltale signs of two types of collisions: elastic collisions between ionic species and charge exchange collisions between ionic species or between ions and neutral particles. Idealized precollision distributions of energy and energy/unit charge are shown in Fig. 2a. Energy is the real quantity of interest, but energy/unit charge is what is measured by the MBMS.

Elastic Collisions (Between an Ion of Charge $q = 1$ and an Ion of Charge $q = n$)

Because these ions will see the same accelerating voltage, their distributions will have maximum energy/charge ratios that will be the same and will be very close to, but less than, the thruster discharge voltage. The minimum energy/charge of the distribution is more difficult to define as it depends on how far the accelerating potential drops within the ionization zone of the thruster. The

Table 1 Thruster operating conditions—cathode flow rate (6 sccm for all cases)

Condition	Discharge voltage, V	Discharge current, A	Total flow rate, sccm	Tank pressure torr
1	300	5.3	64	5.5×10^{-6}
2	500	5.3	64	5.5×10^{-6}

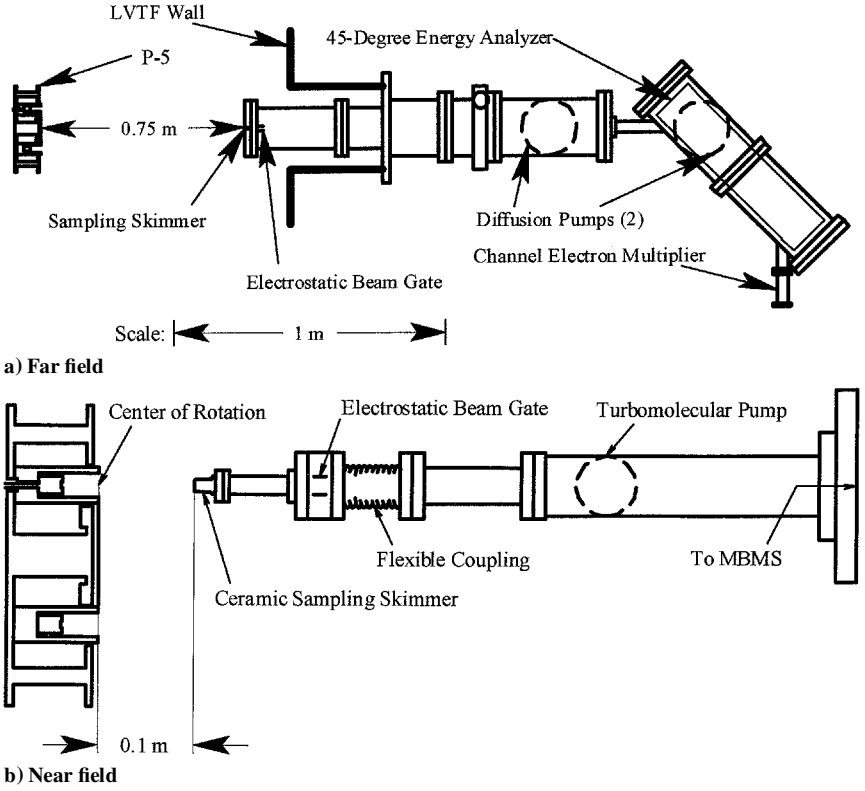

Fig. 1 MBMS configurations.

peaks of both voltage distributions will occur at the same value of energy/charge. Idealized postelastic collision distributions are shown in Fig. 2b. Although elastic collisions between ions and background neutrals do occur, they cannot be detected by the MBMS because they result in a high velocity neutral (which does not respond to the ion-energy filter) and a low (zero) velocity ion (which does to traverse the MBMS). We recognize these collisions based on the following characteristics: 1) a high-voltage tail on the singly charged ion-energy/charge distribution that decays to zero at an energy/charge equal to n times the maximum energy/charge of the ion with charge n (in its precollision distribution); 2) a low-voltage tail on the energy/charge distribution of the ion with charge n that decays to zero at an energy/charge equal to $1/n$ times the minimum energy/charge of the singly charged ion; and 3) these tails decay monotonically without any local maxima.

Charge Exchange (CEX) Collisions

If, for example, a doubly charged ion, accelerated by a potential V (thus energy, $E \sim 2V$ because $E = qeV$), undergoes a CEX collision with a neutral atom (with zero velocity) and one electron is transferred to the doubly charged ion, the resulting singly charged ion would have twice the kinetic energy of a normally produced singly charged ion. Thus, in the energy/charge domain of the measurements of the MBMS, it will appear as a maximum at twice the most probable voltage found in the main distribution. Idealized post-CEX collision distributions are shown in Fig. 2c and have the following characteristics:

1) CEX collisions produce appendages to the main distribution that do not decay monotonically as in the case of elastic collisions.

2) These appendages exhibit local maxima corresponding to the energy distribution of the colliding species.

3) CEX collisions conserve the shape of the original distribution.

4) Ion-neutral CEX collisions only produce detectable ions at energy/charge ratios greater than the original ion, whereas ion-ion CEX collisions can produce detectable ions at energy/charge ratios above and below the original ions (neutral particles produced in these collisions are not detectable by the MBMS).

Ion Energy

Figures 3 and 4 show the far-field ion-energy distributions. All measurements have been corrected for plasma potential, based on Langmuir probe measurements.[1] For the low voltage case (Fig. 3) at 0 deg (centerline), the primary ion-energy distribution has its peak at 255 V with respect to the plasma. The peak is approximately 90% of the discharge voltage, which is what is expected for a well-developed Hall thruster.[13] In this distribution we see strong evidence of elastic collisions between singly and doubly charged xenon ions, decaying at twice the discharge voltage. This behavior is very similar to that observed for the SPT-100. When this distribution is examined more closely on a semilog plot, small CEX collision peaks at 2X and 3X the primary peak are seen. Because there are no CEX peaks at voltages less than the primary peak, these peaks must be the result of CEX collisions by neutrals with doubly and triply ionized xenon that result in singly charged ions. For the high voltage case (Fig. 4) the primary distribution at 0° has its peak at 447 V with respect to plasma. Again, as expected, the peak is approximately 90% of the discharge voltage. In this distribution there is some indication of elastic collisions, seen in the high- and low-energy tails to the primary peak. There are, however, very noticeable ion-neutral CEX collision peaks at 1.5X, 2X, and 3X the primary peak. The 2X and 3X peaks are the result of collisions by neutrals with doubly and triply ionized xenon that result in singly charged ions. The 1.5X peak results from a collision of triply ionized xenon with a neutral that produced a doubly charged ion.

As the thruster is rotated to higher angles, similar trends were seen for all three conditions. For the low voltage case (Fig. 3) the shape of the profile changes very little from 0 to 40 deg. Then at 45 deg the profile begins to broaden significantly toward the lower energy side of the distribution. This trend continues to approximately 50 deg and then transitions into a shift of the primary peak location as seen at 60 deg where the maximum of the primary peak is at 197 V. At angles where this broadening and shift are seen, the ion current intensity is significantly lower than in areas where the distribution has its peak at the same voltage as at 0 deg. Beginning at 65 deg, the profile shifts back to the same shape seen at centerline. The intensity of the signal also increases, though it is far less than at

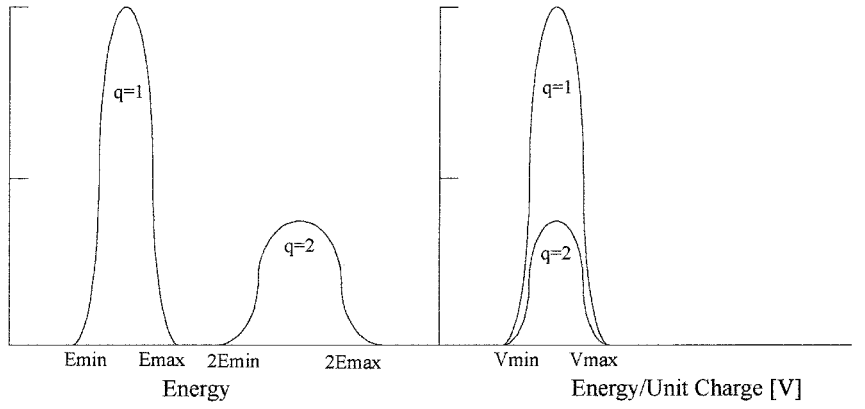

a) Precollision

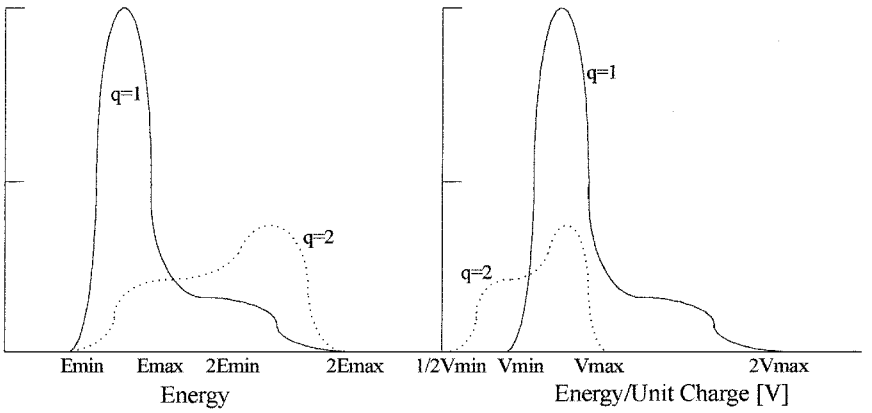

b) Postelastic collision

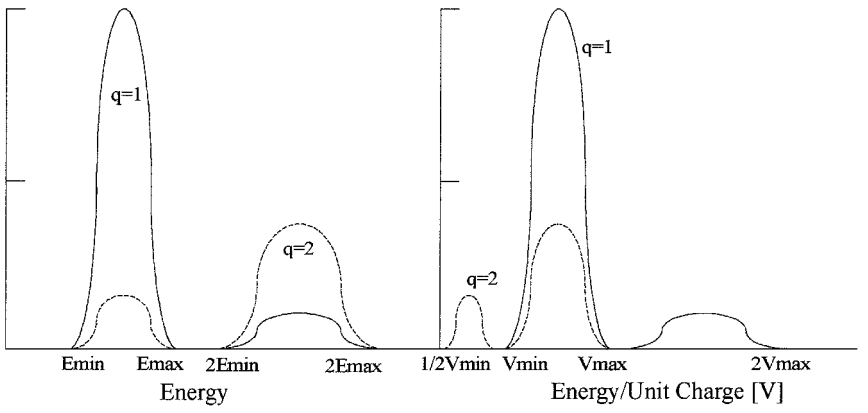

c) Post-CEX collision

Fig. 2 Idealized energy and energy/unit charge distributions.

centerline. The next region begins at approximately 85 deg, where we see evidence of significant numbers of ion-ion CEX collisions and a highly attenuated peak at the centerline voltage. The last signal region occurs at 100 deg, where we see a low-intensity distribution of low-energy ions created outside the discharge chamber. Beyond this, the signal fades into the noise at 105 deg.

For the high voltage case (Fig. 4) the distributions retain the centerline shape only out to 10°. From 15 to 30 deg, the low-energy side of the distribution grows and is accompanied by high-energy CEX collision peaks at 2X and 3X the peak voltage. This then transitions into a peak shift, though it is slightly different than for the low voltage case. From 35 to 50 deg, the primary peak remains and is approximately the same intensity as the shifted peak. At these angles there is also a significant 2X CEX peak. Then, from 60 to 70 deg, the primary peak regains dominance, though the shifted peak remains—in this range, there is no 2X CEX collision peak. The signal then shifts back toward the centerline shape before becoming dominated by high-energy ion-ion CEX peaks at 85 deg. Again there is a low-energy distribution at 100 deg and the signal fades into the noise at 105 deg.

We now proceed to examine the near-field ion-energy distributions, again starting with the 0 deg distributions. In Fig. 5, for the low voltage case, the primary peak at 0 deg again has its maximum at 255 V. In the near field the profile is CEX collision dominated. Upon closer examination, we see peaks at 1.33X, 2X, and 3X the discharge voltage. A peak at 1.33X indicates a CEX collision between a quadruply charged xenon ion and a neutral xenon atom with one electron exchanged. Peaks at 1.5X for triply charged xenon becoming doubly charged and at 4X for quadruply charged xenon are not seen at 0 deg, but are seen from 5 to 15 deg. In Fig. 6, at 0 deg for the high voltage case, the primary peak has a maximum at 448 V. Close examination shows that the profiles are again dominated by CEX collisions. Peaks are observed at 1.33X, 1.5X, 2X, and 3X the primary peak (because of their proximity, the 1.33X and 1.5X peaks tend to blend together into a single "bump" with two maxima). For most of the high voltage sweeps, we observe an increase

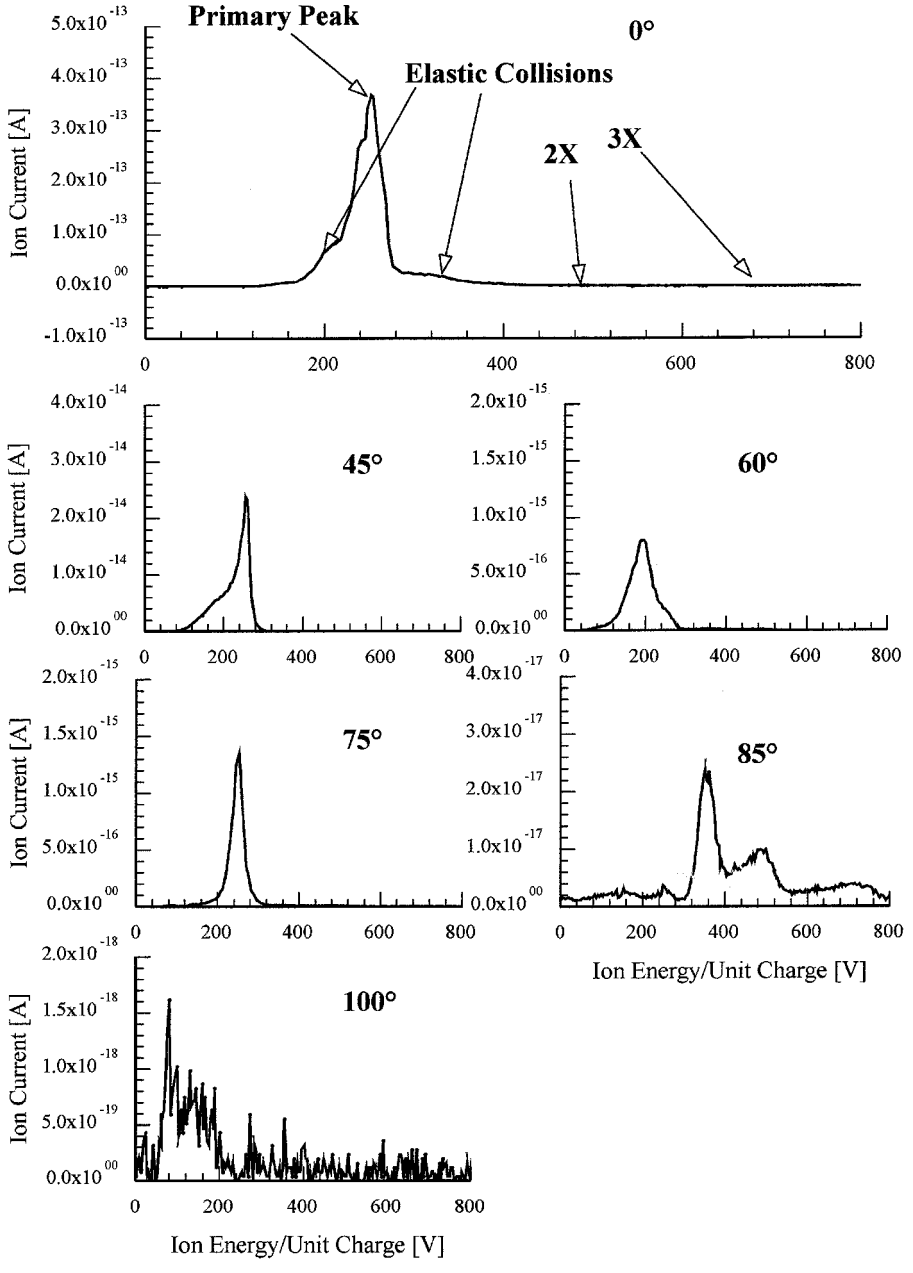

Fig. 3 Far-field ion-energy distributions—low voltage.

in intensity at the end of the scanning range. It is hypothesized that this is the beginning of the peak at 4X the primary peak (~1800 V). Unfortunately, the scanning range of the sourcemeter is not sufficient to encompass this peak in its entirety.

As was seen for far-field measurements, when the thruster is rotated to higher angles, similar trends are observed for both conditions. Figure 5 illustrates the low voltage case. The centerline profile is maintained to 40 deg off centerline. Then from 45 to 55 deg, strong 2X and 3X CEX peaks are observed. From 60 to 85 deg, the CEX peaks remain, but the primary peak at 255 V is attenuated as seen at 70 deg. The primary peak briefly regains dominance at 90 deg, before the signal fades into the noise at 95 deg. For the high voltage case the trends are almost identical, as shown in Fig. 6. The only differences were that the primary peak at 448 V did not attenuate until an angle of 65 deg, instead of 60 deg, and the signal fades into the noise at 90 deg, before the primary peak has an opportunity to reappear.

Time-of-Flight Mass Spectroscopy

Next, we examine the results for species measurements obtained using the time-of-flight configuration of the instrument, beginning with the low voltage far field at 0 deg (Fig. 7). In this trace at the primary peak (255 V), singly, doubly, and triply ionized xenon were observed at an atomic mass-to-charge ratios of 131, 65.5, and 44, respectively. Note that species are identified by the leading edge of a peak, not by its maximum. If the gate is left open for a sufficient amount of time such that the peak is not clipped by the closing of the gate, the intensity is related to the density of a particular species. For a particular accelerating potential, the individual species fraction f_i can be determined using the following equation, where I_i is the signal intensity and q_i is the charge:

$$f_i(V) = \frac{I_i/\sqrt{q_i}}{\sum_i \left(I_i/\sqrt{q_i}\right)} \tag{2}$$

The fractions were determined at various accelerating potentials, as shown in Figs. 8 and 9, along with normalized ion-energy traces taken at 0 deg for reference. They show local maxima of double and triple ion fractions that correspond closely to bumps in the ion-energy distribution, thus confirming their origin as collisional products.

For near-field measurements we again present a trace of the species peaks vs mass for the low voltage case at the maximum

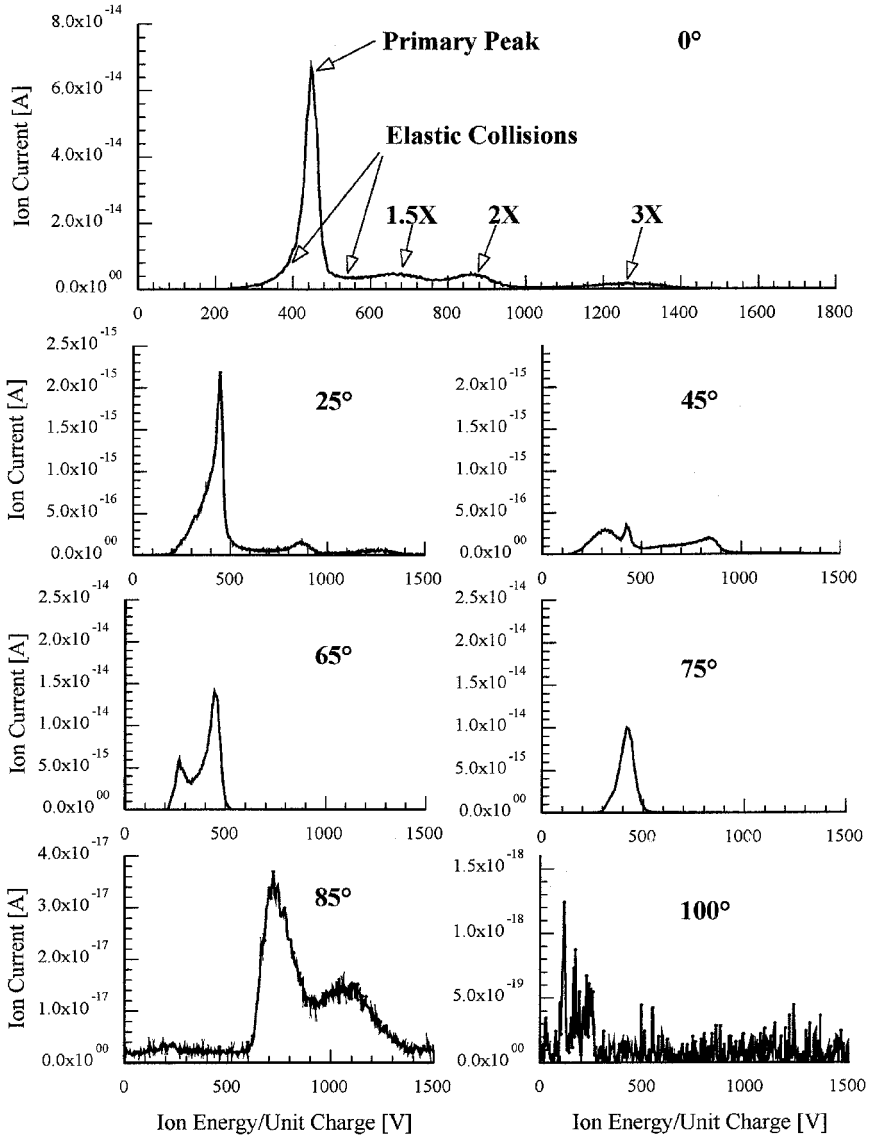

Fig. 4 Far-field ion-energy distributions—high voltage.

Table 2 Species fractions at primary peak (255 V) for low voltage case in the far and near field

	Xe^{+}	Xe^{2+}	Xe^{3+}	Xe^{4+}
Far field: 75 cm	0.92	0.07	0.01	——
Near field: 10 cm	0.63	0.26	0.08	0.03

of the ion-energy distribution (255 V) in Fig. 10. In addition to the ions detected in the far field, we detect the presence of a peak at an apparent mass of 32 amu, which corresponds to the atomic mass-to-charge ratio of quadruply charged xenon. In our near-field ion-energy measurements we detected CEX peaks at 1.33X and 4X the primary discharge peak, which also correspond to quadruply ionized xenon. Thus, these measurements act as an independent confirmation of the presence of Xe^{4+} in the plume. Collisions that remove quadruply ionized xenon from the system are greater in number than those that produce it. By the time a sample is taken 75 cm from the thruster, almost all of the quadruply charged xenon has been converted to a lower charge state ion or neutral, increasing the fraction of these other ions in the process, as shown in Table 2. The measurement uncertainty in these fractions is ±0.6%.

Data Analysis

Examining the changes between the thruster operating conditions, we see very similar trends between the low and high voltage cases, with nearly identical changes in structure with angle. The primary driving force in altering these distributions is changed to the thruster's magnetic field. This laboratory model thruster has inner and outer electromagnet circuits that are controlled independently from each other and from the thruster discharge. The values used for the electromagnet currents were determined during performance measurements and were set to minimize discharge current (thus maximizing efficiency). The resultant ratio of inner-to-outer electromagnet current varied for the various thruster operating conditions. Thus, the inner and outer electromagnets produced different fields for the different operating conditions, changing both the intensity and shape of the overall magnetic field. It is presumed that altering the intensity of the magnetic field in this way also results in an alteration of the shape of the magnetic field and thus the direction of ion acceleration.

In presenting the changes in ion-energy distribution with angle, an attempt to divide the plume into several zones was made. Of course, these zones do not have finite boundaries, and the characteristics seen in them often overlap, thus the zones are created for the purpose of clarity. The angular boundaries of these zones are different for the different operating conditions.

In the far field the first zone is the primary discharge region near 0 deg, as seen in Fig. 3. The ions accelerated in this manner are those created by collisions with electrons trapped around radial or near-radial magnetic field lines in close proximity to the end of the discharge chamber. In other words, these are the ions that are desired

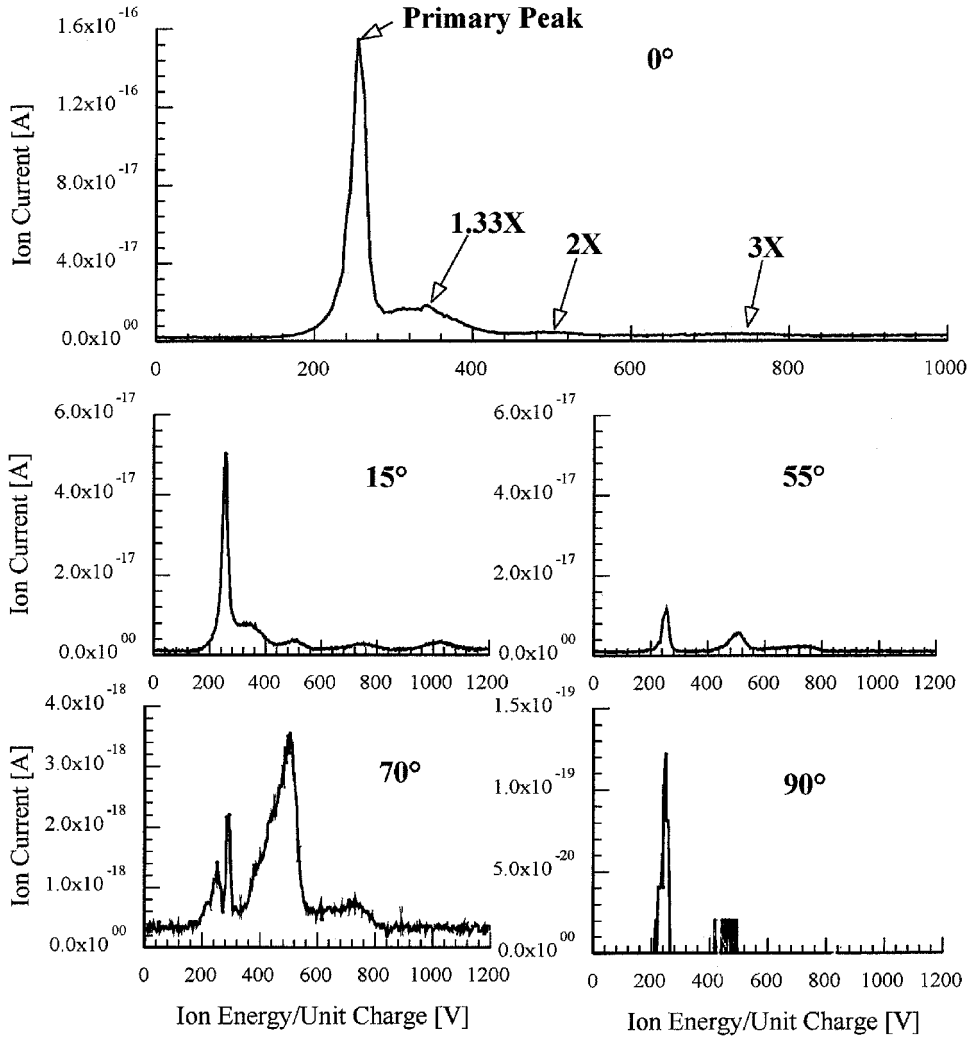

Fig. 5 Near-field ion-energy distributions—low voltage.

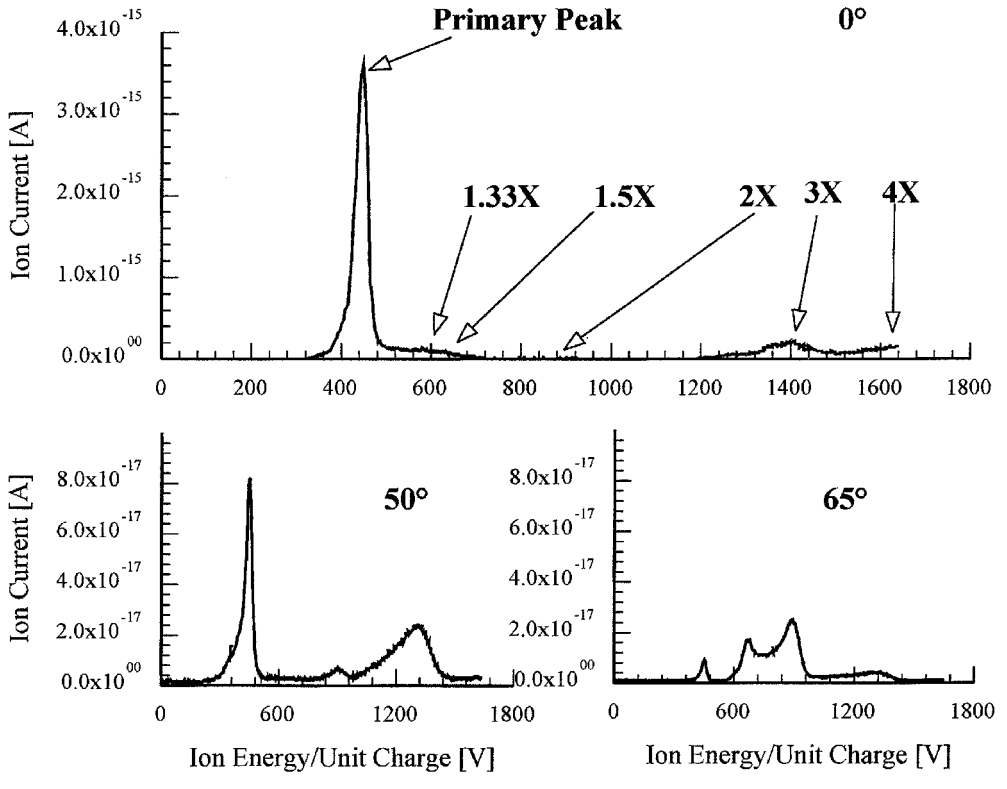

Fig. 6 Near-field ion-energy distributions—high voltage.

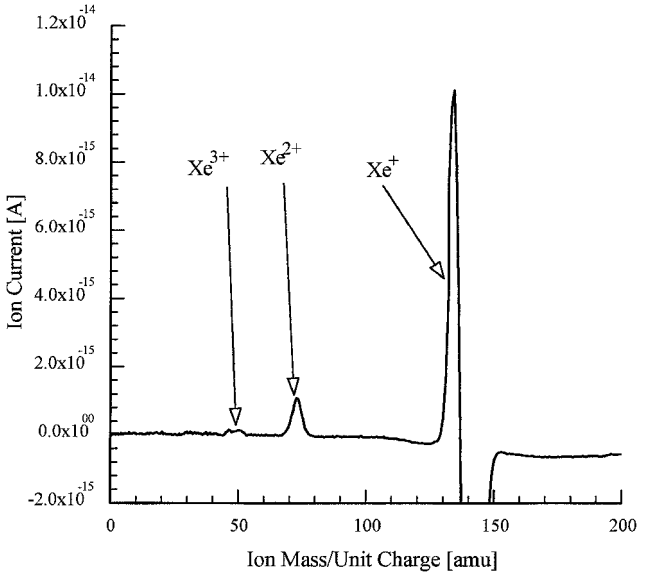

Fig. 7 Far-field time-of-flight peaks for low voltage case—primary voltage (255 V).

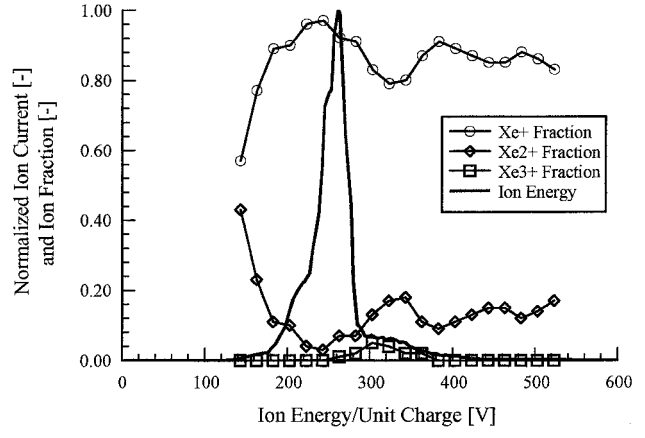

Fig. 8 Far-field ion fractions at low voltage case—0 deg.

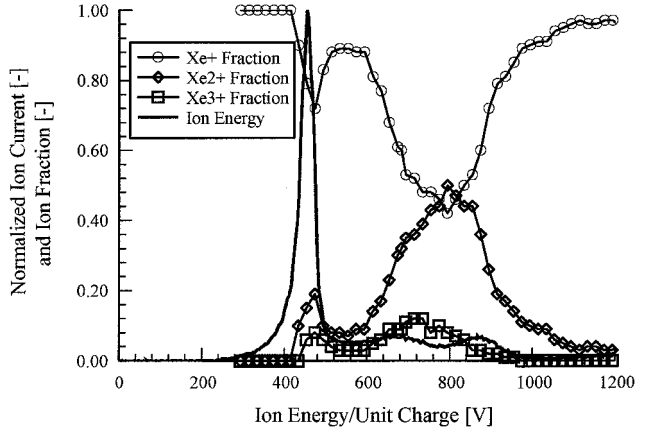

Fig. 9 Far-field ion fractions at high voltage case—0 deg.

in a Hall thruster, which create a majority of the useful thrust. The intensity of peaks in this zone are the highest, thus a majority of propellant ions are concentrated in this zone.

Next in the far field is a low-energy region, typically extending from 40 to 70 deg, with ions that have energy/charge ratios less than the primary peak. They do not, however, have voltages or other characteristics that correspond to CEX collisions. These ions are accelerated outside of the discharge chamber, in regions of low plasma

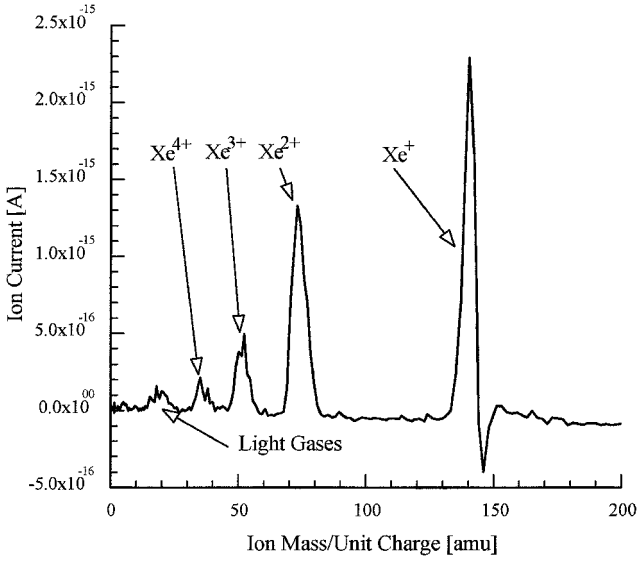

Fig. 10 Near-field time-of-flight peaks for low voltage case—primary voltage (255 V).

potential, where the magnetic field lines have significantly greater curvature than those in the primary discharge region. Thus, ions are accelerated at off-centerline angles with voltages significantly less than the discharge voltage. As will be explained in the near-field section, these ions originate from the far side of the discharge chamber and are accelerated inward, across centerline.

The next two regions, where the profile returns to a centerline-like shape followed by a CEX region, are the most puzzling. In both these regions ions are accelerated by the same potential that the primary discharge regions ions are, but at large angles. It is theorized that the field lines which produce the primary discharge ions are not completely radial, but instead have a sharp curvature on the inward side of the discharge chamber. Ions created in this region will be accelerated normal to the field lines, thus they experience the same accelerating potentials as centerline ions but are directed in the range of 60 to 80 deg with respect to centerline. As the angle is increased toward 90 deg, these ions encounter the acceleration region on the opposite side of the discharge chamber, undergoing large numbers of ion-ion CEX collisions.

Beyond 90 deg, we see a small region of low-energy ions. These are created along magnetic field lines with very large radii, such that they curve beyond 90 deg and accelerate the ions backwards with respect to the desired thrust vector. The energy of these ions is low, because they were created along a field line that is relatively far outside the discharge chamber. Ions are not seen at angles significantly beyond 90 deg because the P5's magnetic pole pieces are wide and block their acceleration.

In the near field we see, as expected, the primary discharge region near centerline (see Fig. 5). Going outward in the plume, we do not see the low-energy region that was seen in the near field. However, looking at the thruster orientation, we realize that with the sampling orifice centered on the annular discharge chamber (see Fig. 2), ions from the far side cannot enter the orifice, except at high angles. However, high-angle inwardly directed particles, those that are responsible to the return to centerline and CEX regions in the far-field as seen in Fig. 3 at 75 and 85 deg, respectively, can enter the orifice, resulting in ion-energy distributions like those shown in Fig. 5 at 55 and 70 deg. This behavior continues to dominate all of the way out to loss of signal.

If the ion-energy distributions observed at angles outside the primary discharge region were the result of ions travelling radially outward from the discharge chamber, then there should be very little variation in their shape because at all angles the plasma would be undergoing CEX collisions with the uniform background neutral gas. However, if the ions are travelling radially inward, we expect much greater variation because the plasma would be encountering

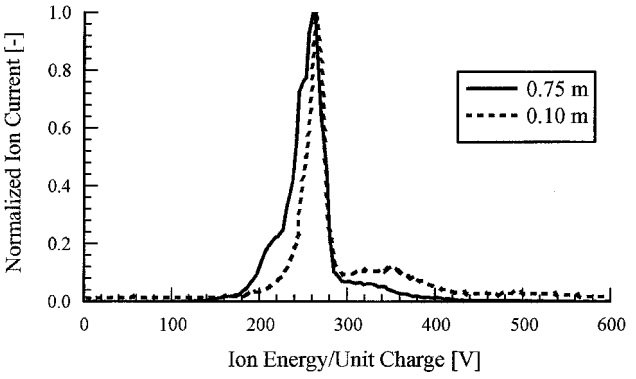

Fig. 11 Normalized ion-energy profiles—0 deg.

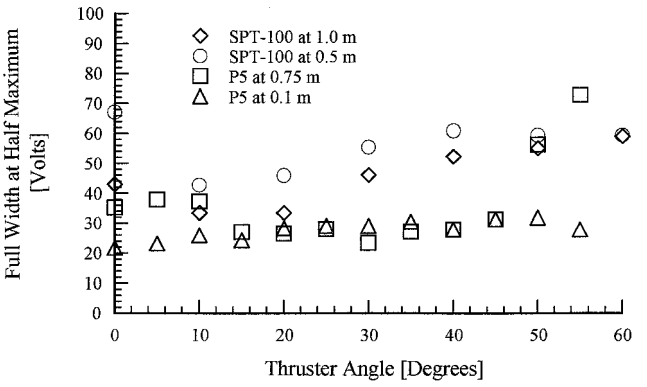

Fig. 12 Full width at half maximum—low voltage case and SPT-100.

ions and neutrals from the other side of the annulus, the density of which will increase with angle. This appears to be what was observed in this investigation. For this to be correct, however, the density must be high enough that the mean free path for ion-neutral CEX collisions is on the order of (or less than) the diameter of the discharge chamber (~15 cm). Measurements taken inside of a D-55 Hall thruster[14] indicate pressures on the order of 1 m torr for equivalent flow rates. Calculations for the P5 also indicate a neutral pressure of approximately 1 m torr based on a neutral temperature of 1000 K and a neutral velocity of 300 m/s. At these pressures the ion-neutral CEX collision mean free path[15] was determined to be 5 cm. Though influences outside the discharge chamber, such as the cathode or other structures, will affect the neutral density, this simple analysis shows that ion-neutral CEX collisions are statistically likely in this region. Therefore, it appears that most of the ions produced by this thruster are either accelerated axially along the thrust vector or have an inwardly directed radial component, toward the thruster centerline. Langmuir probe measurements taken inside the discharge chamber using a high-speed reciprocating probe support this conclusion.[16] These measurements show plasma equipotential lines that curve back toward the anode in the inner portion of the discharge chamber. Because ions are accelerated perpendicular to equipotential lines, they will travel inward, across thruster centerline.

When we compare individual near-field ion-energy traces to those taken in the far field, we see a number of differences. Figure 11 shows the 0-deg ion-energy profiles for the low voltage case in the near field and far field. They have been normalized and overlaid for comparative purposes. The first thing that we notice is that the trace taken at 10 cm is significantly narrower than that taken at 75 cm. The full width at half maximum in the near field was 22 V, as compared to 35 V in the far field. The increased width appears as low-energy elastic collisions. We also see that the 1.33X CEX collision observed at 10 cm has disappeared by 75 cm. In general, elastic collisions are far more prevalent in the far field than in the near field, obscuring CEX collisions in some cases. This is as expected because, for ions of the energy range found in the Hall thruster,[17] CEX collisions are approximately an order of magnitude more likely than elastic collisions. Thus, by sampling close to the thruster, the probability of CEX collisions is reduced, from 7.9% at 75 cm to 1.1% at 10 cm (Ref. 12).

Figure 12 shows the full width at half-maximum measured at near and far field for the low voltage case, with a comparison to SPT-100 data. The narrowing of these ion-energy profiles compared to the SPT-100 is a result of the improvements made to the chamber pumping capacity through the installation of cryopumps. With lower background pressure the frequency of pressure broadening causing collisions is reduced, and thus the profiles are narrower at low angles. We see that the full width at half maximum is broadened in the far field at low and high angles. As already discussed, at high angles inwardly directed low-energy ions cross over the centerline and collide with the flow from the other side of the discharge chamber. These collisions result in the broadening of the ion-energy distribution. At low angles the conjecture was that when the thruster was firing directly toward the sampling skimmer plasma from the thruster that does not enter the orifice impacts on the surrounding flange and is neutralized. This would represent a localized area of high-pressure neutral xenon that would cause collisions and broaden the profile. This hypothesis was checked by placing a neutral particle flux probe[18] just below the sampling orifice, perpendicular to the flow. These measurements indicated a marked increase in pressure within 20 deg of centerline, the same region where the far-field full width at half maximum measurements show broadening. Therefore, based on these results, we believe that the low-angle broadening in the full width at half maximum is primarily a facility effect, whereas the high-angle broadening is the results of collisions caused by crossover flow.

Comparison with Laser-Induced Fluorescence

The University of Michigan laser-induced fluorescence (LIF) system was used to investigate the ion-energy profile of the P5.[19] Measurements were taken at the low voltage case, 10 cm downstream of the exit plane. At the center of the discharge chamber, the axial velocity was measured to be 16,700 m/s. This is approximately 87% of the velocity, 19,250 m/s, calculated based on the peak ion-energy distribution at the same location (see Fig. 5). The axial ion temperature at this point was 0.75 eV, whereas the full width at half-maximum spread in ion energy measured by the MBMS was 21 V. However, analysis has shown that these two methods are reporting different, but related, ion-energy quantities.[20] LIF measurements report the random spread in ion energy, the ion temperature, while MBMS measurements give the spread in ion energy resulting from ion acceleration over a potential spread. When the proper transformations are applied, the ion-energy quantities from the two experimental techniques agree reasonably well.

Summary

In summary, we have used ion-energy diagnostics and time-of-flight mass spectroscopy to show the evidence of singly, doubly, triply, and quadruply charged xenon within the plume of the P5. We have used measurements of the ion-energy distribution at various angles and axial locations to determine the ion acceleration structure of the thruster and show that the shape and magnitude of the magnetic field drive this structure, focusing the plasma inward. We have seen that sampling the plasma closer to the thruster gives a profile that has undergone fewer structural changes because of collisions within the plume and with background neutrals within the test facility. This method should be of great use in all aspects of thruster design and research. Thruster integrators can use the method to create a straightforward map of ion concentration, energy, and charge state that will enable them to understand the implications of placing a Hall thruster (or other electric propulsion device) on their spacecraft. Additionally, by making measurements at multiple axial points, we obtain an understanding of the ion acceleration process. This will allow thruster designers the opportunity to examine the effect that changes that they make in thruster configuration (e.g., magnetic configuration, accelerating potential, etc.) have on the ion acceleration structure. These ion vector measurements should also

be valuable to thruster modelers because it will allow them to compare their ion acceleration structures directly with those determined experimentally. Finally, it is noted that the differences seen between LIF ion energy data and data from other sources are the result of differences in terminology.

References

[1]Haas, J. M., Gulczinski, F. S., Gallimore, A. D., Spanjers, G. G., and Spores, R. D., "Performance Characteristics of a 5 kW Laboratory Hall Thruster," AIAA Paper 98-3503, July 1998.

[2]Arkhipov, B., Bober, A., Day, M., Gnizdor, R., Kozobsky, K., and Maslennikov, N., "Extending the Range of SPT Operation: Development Status of 300 and 4500 W Thrusters," AIAA Paper 96-2708, July 1996.

[3]Garner, C. E., Trendokhlebov, S. O., Semenkin, A. V., and Garkusha, V. I., "Evaluation of a 4.5 kW D-100 Thruster with Anode Layer," AIAA Paper 96-2967, July 1996.

[4]Petrosov, V. A., et al., "Investigation 4.5 kW High Efficiency Hall Type T-160 Electric Thruster," IEPC Paper 95-03, Sept. 1995.

[5]Randolph, T., Pencil, E., and Manzella, D., "Far Field Plume Contamination and Sputtering of the Stationary Plasma Thruster," AIAA Paper 94-2855, July 1994.

[6]Roussel, J. F., Bernard, J., and Garnier, Y., "Numerical Simulation of Induced Environment, Sputtering, and Contamination of Satellite Due to Electric Propulsion," *Proceedings of the 2nd European Spacecraft Propulsion Conference*, May 1997 (ESA SP-398, Aug. 1997).

[7]Manzella, D. H., "Stationary Plasma Thruster Plume Emissions," Electric Rocket Propulsion Society, IEPC Paper 93-097, Sept. 1993.

[8]Vahrenkamp, R. P., "Measurement of Double Charged Ions in the Beam of a 30-cm Mercury Bombardment Thruster," AIAA Paper 73-1057, Oct. 1973.

[9]Hutchinson, I., *Principles of Plasma Diagnostics*, Cambridge Univ. Press, New York, 1987, pp. 79–84.

[10]King, L. B., and Gallimore, A. D., "Ion-Energy Diagnostics in the Plasma Exhaust of a Hall Thruster," *Journal of Propulsion and Power*, Vol. 16, No. 5, 2000, pp. 50, 51.

[11]Dushman, S., *Scientific Foundations of Vacuum Technique*, Vol. 4, Wiley, New York, 1958.

[12]Gulczinski, F. S., "Examination of the Structure and Evolution of Ion Energy Properties of a 5 kW Class Laboratory Hall Effect Thruster at Various Operational Conditions," Ph.D. Dissertation, Dept. of Aerosapce Engineering, Univ. of Michigan, Ann Arbor, Dec. 1999.

[13]Zhurin, V. V., Kaufman, H. R., and Robinson, R. S., "Physics of Closed Drift Thrusters," Electric Rocket Propulsion Society, IEPC Paper 97-191, Aug. 1997.

[14]Marrese, C. M., Polk, J. E., King, L. B., Garner, C., Gallimore, A. D., Semenkin, S., Trendokhlebov, S., Garkusha, V. I., "Analysis of Anode Layer Thruster Guard Ring Erosion," Electric Rocket Propulsion Society, IEPC Paper 95-196, Sept. 1995.

[15]Rapp, D., and Francis, W., "Charge Exchange Between Gaseous Ions and Atoms," *Journal of Chemical Physics*, Vol. 37, No. 11, 1962, pp. 2631–2645.

[16]Haas, J. M., Hofer, R. R., and Gallimore, A. D., "Hall Thruster Characterization Using a High-Speed Axial Reciprocating Electrostatic Probe," AIAA Paper 99-2425, June 1999.

[17]Brown, S. C. (ed.), *Basic Data of Plasma Physics*, American Inst. of Physics Press, New York, 1994, pp. 31–34.

[18]Marrese, C. M., Gallimore, A. D., Spindt, C., Polk, J. E., Goodfellow, K. D., and Jensen, K. L., "Field Emission Array Cathodes for Electric Propulsion Systems," AIAA Paper 98-3484, July 1998.

[19]Williams, G. J., Smith, T. B., Gulczinski, F. S., Beal, B. E., Gallimore, A. D., and Drake, R. P., "Laser Induced Fluorescence Measurement of Ion Velocities in the Plume of a Hall Effect Thruster," AIAA Paper 99-2424, June 1999.

[20]Williams, G. J., Smith, T. B., Gulczinski, F. S., Gallimore, A. D., and King, L. B., "Correlating Laser Induced Fluorescence and Molecular Beam Mass Spectrometry Ion Energy Measurements," (to be published).